Check for updates

Hyaluronic acid-loaded drug-eluting nanofibrous pad for the treatment of degenerative arthritis

Yung-Heng Hsu,[a] Pin-Chao Feng,[bc] Yi-Hsun Yu,[a] Ying-Chao Chou,[a] Zhe-Pei Wang[b] and Shih-Jung Liu 🆔 *[ab]

Despite advancements in modern technology, treating degenerative arthritis remains a challenge. This study developed a degradable, hyaluronic acid-loaded, drug-eluting nanofibrous pad designed to provide extended pain relief and prevent infection at the knee joint. The mechanical performance of the biodegradable pads was assessed, and the pharmaceutical discharge kinetics were estimated using an *in vitro* elution method. Additionally, *in vivo* pharmaceutical release and efficacy were tested using a rabbit activity model. The experimental results suggest that the degradable pad exhibited strong mechanical properties. *In vitro*, the drug-eluting nanofibrous pad sustained the release of teicoplanin, ceftazidime, and ketorolac for 10, 24, and 30 days, respectively, and maintained high levels of connective tissue growth factor elution over a 30-day period. Moreover, animal testing demonstrated that the pad released significant amounts of antimicrobial and pain-relieving agents in a rabbit knee joint model for over 28 days. Rabbits implanted with the drug-eluting pads exhibited activity levels comparable to those that did not undergo surgery. These findings indicate that the hyaluronic acid-loaded, drug-eluting nanofibrous degradable pad, with its extended release of pharmaceuticals and biomolecules, may be used for the treatment of degenerative arthritis.

1 Introduction

Osteoarthritis is a progressive joint disorder marked by cartilage deterioration, resulting in pain, stiffness, and limited mobility. It primarily affects weight-bearing joints like the knees, hips, and spine, with its incidence rising with age. Osteoarthritis treatment focuses on relieving symptoms, slowing disease progression, and enhancing the patient's quality of life.[1-3] Non-pharmacological approaches include exercise, physical therapy, weight management, and assistive devices. Pharmacological treatments may involve over-the-counter pain relievers, nonsteroidal anti-inflammatory drugs, corticosteroid injections, and hyaluronic acid injections to improve joint lubrication. In severe cases, surgical procedures such as arthroscopy, osteotomy, or joint replacement may be required to replace or reconstruct damaged joints to restore functionality.[4-6]

Despite advances in modern technology, the repair of degenerated cartilage presents a significant challenge in orthopedics and regenerative medicine. Various approaches

have been explored to address this issue, ranging from surgical interventions to tissue engineering strategies. Surgical procedures such as microfracture, mosaicplasty, and autologous chondrocyte implantation involve stimulating the body's natural healing response or transplanting healthy cartilage tissue to the damaged area.[7-9] However, these techniques have limitations in terms of long-term efficacy and the ability to regenerate functional cartilage tissue. Tissue engineering approaches aim to create bioengineered cartilage constructs using combinations of biomaterials, drugs, and growth factors to mimic the structure and function of native cartilage.[10,11] Advances in biomaterial science hold promise for developing novel therapies for cartilage repair. However, further research is needed to optimize these approaches and translate them into clinically effective treatments for degenerated cartilage.

In this work, degradable drug-eluting pads were developed for potential therapy for degenerative arthritis. A hyaluronic acid-loaded polycaprolactone (PCL) pad was manufactured using a specially designed mold, while teicoplanin, ceftazidime, ketorolac, and connective tissue growth factor embedded poly(lactic-*co*-glycolic acid) (PLGA) nanofibers were fabricated through electrospinning and co-electrospinning processes. Hyaluronic acid (HA) is a high-molecular-weight, non-sulfated glycosaminoglycan that serves as a crucial component of the extracellular matrix (ECM) and a biodegradable polymer. Its molecular weight variations allow for the development of diverse formulations, including fillers, creams, gels, and

[a]Department of Orthopedic Surgery, Bone and Joint Research Center, Chang Gung Memorial Hospital-Linkou, Taoyuan 33305, Taiwan. E-mail: shihjung@mail.cgu.edu.tw

[b]Department of Mechanical Engineering, Chang Gung University, 259 Wen-Hwa 1st Road Kwei-Shan, Taoyuan 33302, Taiwan. Fax: +886-3-2118558; Tel: +886-3-2118166

[c]Department of Thoracic and Cardiovascular Surgery, Chang Gung Memorial Hospital-Linkou, Taoyuan 33305, Taiwan

drops.[12–15] PCL is a resorbable polyester characterized by a low melting point of approximately 60 °C and a glass transition temperature near −60 °C. The polymer degrades through the hydrolysis of its ester linkages under physiological conditions, making it suitable for use as an implantable biomaterial.[16,17] Additionally, PLGAs are one of the most extensively studied biodegradable polymers among various biomaterials, primarily because of their adaptability, customizable degradability, and outstanding biocompatibility. PLGA-derived systems have been thoroughly explored for their ability to target specific sites and provide controlled delivery of micro- and macromolecules.[18–20]

Teicoplanin is an antibiotic used to prevent and treat severe infections caused by Gram-positive bacteria, including methicillin-resistant *Staphylococcus aureus* (MRSA) and *Enterococcus faecalis*.[21] Ceftazidime, a member of the cephalosporin class, is typically administered intravenously or intramuscularly. It exhibits a broad *in vitro* spectrum of activity against both Gram-positive and Gram-negative aerobic bacteria, with notable efficacy against Enterobacteriaceae (including beta-lactamase-positive strains), and is resistant to hydrolysis by most beta-lactamases.[22] Ketorolac is a nonsteroidal anti-inflammatory drug (NSAID) delivered *via* IV or IM injection, used effectively as an analgesic either alone or in combination with other drugs in a multimodal pain management approach.[23] Connective tissue growth factor (CTGF) is a crucial regulatory molecule that plays a role in various biological processes such as cell proliferation, angiogenesis, wound healing, and is implicated in conditions like tumor progression and tissue fibrosis.[24]

Electrospinning is a method that uses electrohydrodynamic processing of polymer solutions, offering a potential alternative for encapsulating sensitive bioactive agents with promising applications.[25,26] In this procedure, the solution is charged through a nozzle linked to a high-voltage source. The electrostatic force created by the charges overcomes the surface tension of the solution, causing the solution jet to spin into extremely fine fibers. On the other hand, co-axial electrospinning is a modification of the electrospinning process that involves the arrangement of multiple solution feed systems to simultaneously spin two or more polymer solutions from co-axial capillaries. This method is widely employed to enclose drugs and growth factors within the core of fibers. Unlike surface modification, which only impacts the scaffold surface, co-axial electrospinning allows biological signals to be incorporated throughout the entire scaffold structure, enabling sustained release over a controlled period.[27]

After fabrication, the mechanical properties of the PCL pads were evaluated. The morphological structure of the electrospun and co-electrospun nanofibers was evaluated using scanning electron microscopy (SEM) and transmission electron microscopy (TEM). The presence of antimicrobial agents and analgesics within the nanofibers was verified through Fourier-transform infrared spectroscopy (FTIR) and differential scanning calorimetry (DSC). The release profiles of the pharmaceuticals from the nanofibers were assessed using an elution method and high-performance liquid chromatography (HPLC), while the release of CTGF was measured by enzyme-linked immunosorbent assay (ELISA). Furthermore, the *in vivo*

release patterns of the incorporated pharmaceuticals from the drug-eluting pads were evaluated using a rabbit knee joint model. Additionally, the efficacy of the implanted pads was assessed using an animal behavior cage. Finally, histological assays were conducted.

2 Materials and method

2.1 Resorbable polymers, solvents, pharmaceuticals and biomolecule

Bioresorbable polymers utilized in this work included PCL (Mw: 80 kDa), hyaluronic acid (M_w: 600–1200 kDa), and 50 : 50 PLGA (M_w: 24–38 kDa). The solvents employed were dichloromethane (DCM) and hexafluoroisopropanol (HFIP). The adopted drugs involved teicoplanin, ceftazidime, and ketorolac, and the biomolecule was connective tissue growth factor (CTGF). All substances were acquired from Sigma-Aldrich (Saint Louis, MO, U.S.A.).

2.2 Fabrication of hyaluronic acid loaded PCL pad

An aluminum mold was designed and developed. Fig. 1A displays the layout and dimensions of the mold, comprising two halves with a football-like cavity. To produce the hyaluronic acid-loaded pad, PCL (2.5 g) was initially dissolved in DCM (either 4 mL or 7 mL). A thin layer of the solution was then applied to the inner surface of each mold half. As the DCM
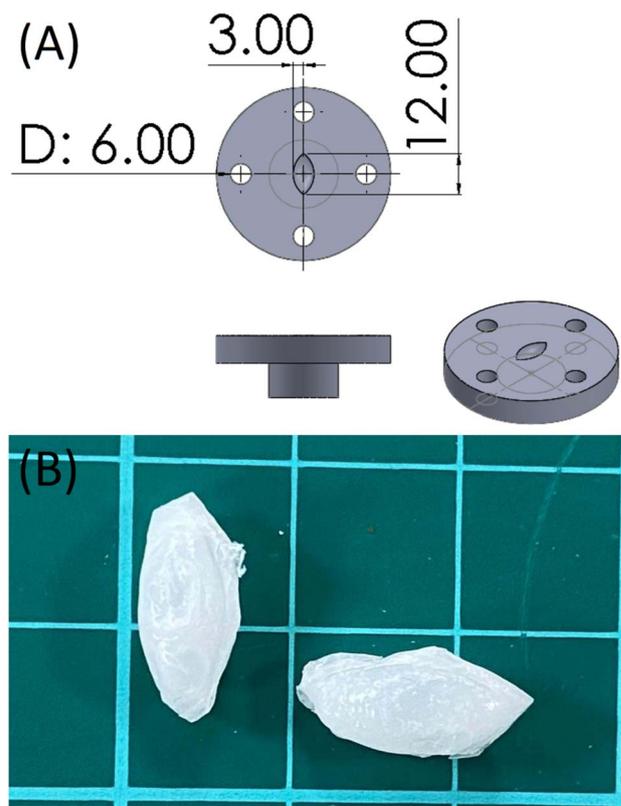

Fig. 1 (A) Layout and dimension of the mold for fabricating the pad, (B) photo of hyaluronic acid loaded pads. (unit: mm).

evaporated, two PCL half shells formed on the mold halves. Following the addition of hyaluronic acid, the two half shells were sealed using another PCL solution (PCL/DCM of 2.5 g/3 mL) as the sealant at the shell interfaces. Subsequently, a football-like hyaluronic acid-loaded pad was obtained (Fig. 1B).

2.3 Electrospinning and co-electrospinning of drugs and biomolecule embedded nanofibers

For the preparation of drugs loaded nanofibers, teicoplanin (93.3 mg), ceftazidime (93.3 mg), and ketorolac (93.3 mg) were blended with PLGA of 800 mg and HFIP of 5 mL. Subsequently, the mixture was electrospun using a lab-made spinning device.[28] The voltage, the flow rate of the mixture, and the distance from the needle to the collection plate were 18 kV, 0.2 mL h^{-1}, and 15 cm, respectively.

To create the CTGF-incorporated sheath-core structured nanofibers, a specialized co-axial device that simultaneously delivers two solutions was employed.[29] PLGA (840 mg) was dissolved in 3 mL of HFIP to serve as the sheath material, while the core solution consisted of 20 μg of CTGF mixed with 1 mL of phosphate-buffered saline. The PLGA and CTGF solutions were put in different feeding needles for co-axial electrospinning. During the co-spinning procedure, the solutions were delivered to the collecting plate at a volumetric flow rate of 0.9 mL h^{-1} for the PLGA shell solution and 0.3 mL h^{-1} for the CTGF core solution, using two independently controlled pumps. The voltage was set to 18 kV, and the distance from the needle to the collecting plate was kept at 15 cm.

All spinning tests were completed at ambient temperature. The thickness of the integrated spun and co-spun bi-layered nanofibers was approximately 0.2 mm, with each layer measuring around 0.1 mm. The spun nanofibers were then placed in an isothermal vacuum oven at 40 °C for 72 hours to evaporate the solvent, after which they were wrapped around the surface of the PCL pad, resulting in the formation of degradable drug-eluting pads.

2.4 Compression tests

The compression strength of the hyaluronic acid-loaded pads was evaluated using a Lloyd tester (Ametek, Berwyn, PA, U.S.A.) fitted with a 2500 N load cell. The pads were positioned between two compression disks, each with a 30 mm diameter. The top disk's downward speed was set to 60 mm min^{-1}, and both the load and deformation were recorded. Each test was conducted in triplicate ($N = 3$).

2.5 Microscopic evaluations of nanofibers

Electrospun drugs loaded nanofibers and co-eletrospun CTGF incorporated nanofibers were coated with gold and examined under a field-emission SEM (JEOL Model JSM-7500F, Tokyo, Japan). The fiber size distribution was analyzed from 50 randomly selected nanofibers.

2.6 Wetting angles

The contact angles of pristine PLGA and PLGA nanofibers incorporated with drugs and biomolecules were measured using a water contact angle analyzer (First Ten Angstroms, USA). Distilled water was carefully dropped onto the surfaces of the nanofibrous samples, and the angles were observed using a video monitor ($N = 3$).

2.7 FTIR assay

The spectra of pristine PLGA and drug-loaded PLGA nanofibers were analyzed using FTIR spectrometry. The measurements were conducted on a Nicolet iS5 spectrometer (Thermo Fisher Scientific, Waltham, MA, U.S.A.) with a resolution of 4 cm^{-1} and 32 scans. The nanofiber samples for analysis were compressed into KBr discs, and spectra were recorded in the range of 400–4000 cm^{-1}.

2.8 Differential scanning calorimetry

The thermal properties of pristine PLGA and pharmaceutical-loaded PLGA nanofibers were evaluated using differential scanning calorimetry (DSC) (Model DSC25, TA Instruments, New Castle, DE, USA). The temperature range for the scan was set from 30 °C to 250 °C, with a heating rate of 10°C min^{-1} for the specimens.

2.9 *In vitro* discharge of pharmaceuticals and biomolecules

The release profiles of teicoplanin, ceftazidime, ketorolac, and CTGF from the nanofibers were assessed using an *in vitro* elution method. Nanofibrous samples (one per test tube, $N = 3$) were placed in glass test tubes holding phosphate buffer solution (PBS, 0.15 mol L^{-1}, pH 7.4) of 1 mL. The tubes were subsequently incubated at 37 °C for 24 hours, after which the eluent was gathered and assayed. New PBS (1 mL) was included for the subsequent 24-hour period, and this process was repeated for 30 days. The drug levels in the eluents were assessed employing high-performance liquid chromatography (HPLC) on a Hitachi L-2200R multi-solvent delivery system (Hitachi High-Technologies Corporation, Tokyo, Japan). CTGF levels were measured using enzyme-linked immunosorbent assay (ELISA). All experimental tests were conducted in triplicate ($N = 3$).

2.10 *In vivo* animal study

Nine New Zealand rabbits (weighing 2500–3000 g) were enrolled, in compliance with the regulations set by the National Institute of Health of Taiwan. The entire procedures gained approval from the Institutional Animal Care and Use Committee (IACUC Approval No.: CGU108-120) of Chang Gung University. Prior to implantation, the drug/growth factor-incorporated nanofibers were wrapped around the surface of the PCL pad. The animals were anesthetized with isoflurane inhalation, maintained with a mask throughout the surgical procedure. After sedation, arthrotomy of the right knee was performed (Fig. 2A). The drug/biomolecule-loaded PCL pad was then implanted into the right knee joint (Fig. 2B), and the
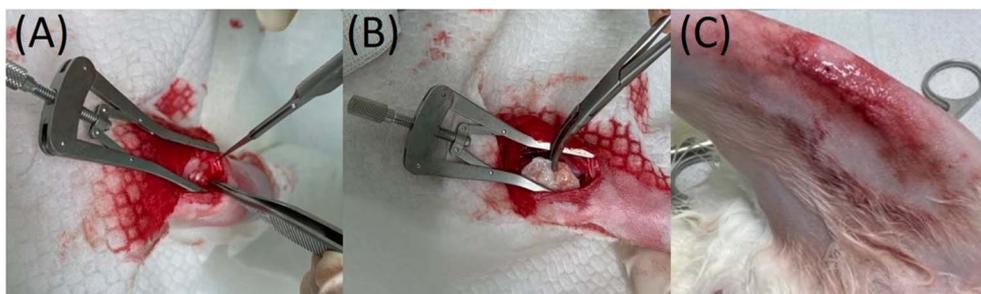
Fig. 2   The surgical procedure: (A) exposing the knee joint, (B) implanting the drug-eluting pad, and (C) closing the wound.

surgical wound was closed (Fig. 2C). *In vivo* drug concentrations were evaluated by collecting tissue/fluids from the surgical site at 1, 3, 7, 14, 21, and 28 days post-surgery, and the samples were assayed by HPLC ($N = 3$).

After operation, each animal was placed in a laboratory-designed cage (Fig. 3) to monitor post-operative activity. The cage, which measures 120 cm × 120 cm × 60 cm, was separated into nine equal square sections. On top of each section, a diffusion-scan photoelectric switch sensor was installed. When an animal migrated from one section to another, the associated sensor was activated. The total number of activations was monitored and recorded over a 7-day period, after which the animal was returned to its initial cage for ongoing care. The activity counts of three groups of animals were evaluated ($N = 3$): the drug-eluting pad group (rabbits receiving surgery and the implantation of drug/biomolecule-loaded pads), the surgery-only group (rabbits undergoing surgery only), and the healthy group (rabbits not undergoing surgery).
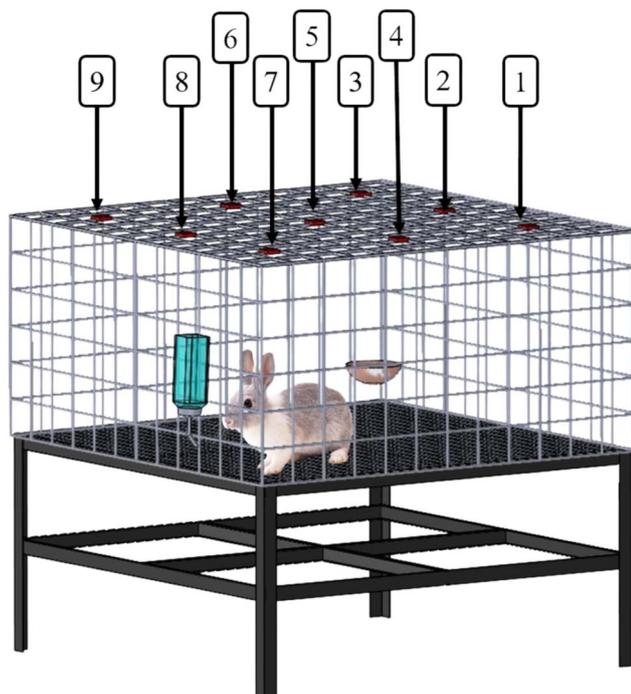
Additionally, histological analyses were performed on tissue samples collected from the suprapatellar pouch of the knee joint at 1, 7, 14, and 28 days post-surgery, followed by hematoxylin and eosin (H&E) staining.

2.11 Statistics analysis

Data are presented as mean ± standard deviation. ANOVA with post hoc corrections was used to analyze the data and assess statistical differences. A *p*-value of less than 0.05 was considered statistically significant.

3 Results

3.1 Drug/biomolecule-eluting hyaluronic acid loaded pads

HA-loaded PCL pads were successfully prepared, with a shell thickness of 298 ± 13 μm. Fig. 4 illustrates the load–deformation curves for pads with different PCL : DCM ratios (either 2.5 g/7 mL or 2.5 g/4 mL, w/v). Clearly, the PCL : DCM ratio did not show an obvious influence on the strength of the prepared pads, with both pads exhibiting highest compressional strength of approximately 25 N.

Fig. 5 displays the morphology and fiber size dispersion of pristine PLGA and drug- and CTGF-loaded PLGA nanofibers.
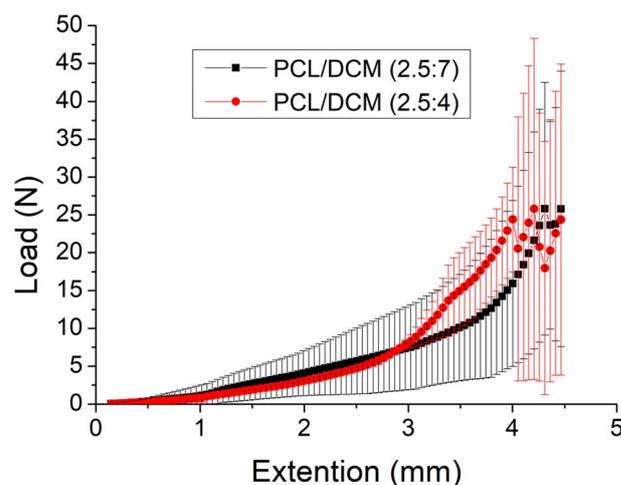

Fig. 3   The cage used to evaluate the animals' activities post-operation.

Fig. 4   Load–deformation curve of hyaluronic acid loaded PCL pads fabricated with different PCL/DCM ratios (either 2.5 g/4 mL or 2.5 g/7 mL).

© 2025 The Author(s). Published by the Royal Society of Chemistry
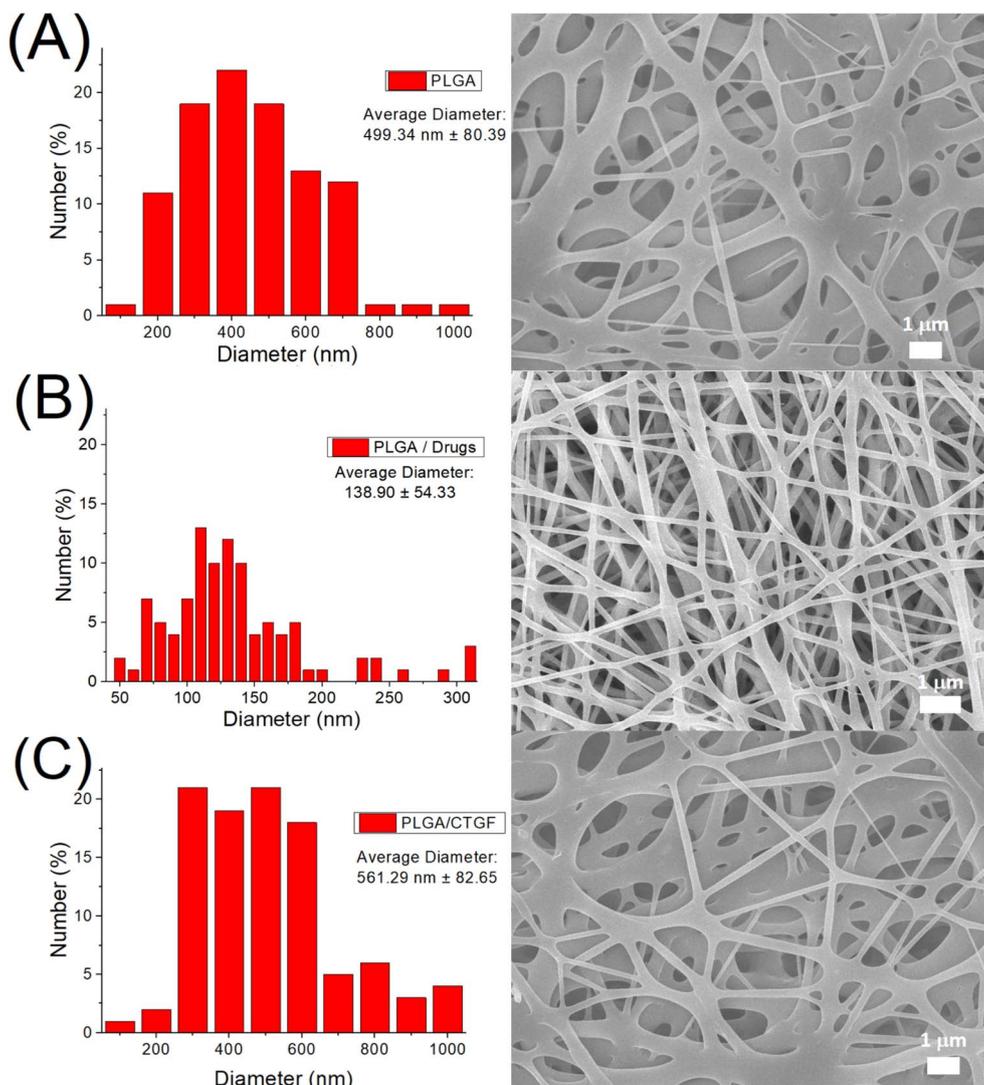
Fig. 5 SEM images and fiber partice size distribution of electrospun (A) pure PLGA nanofibers, (B) drugs loaded nanofibers, (C) CTGF incorporated sheath-core nanofibers.

The average diameters of the spun pristine PLGA nanofibers, drug-embedded PLGA nanofibers, and CTGF-incorporated nanofibers were found to be 499.3 ± 80.4 nm, 138.9 ± 54.3 nm, and 561.3 ± 82.7 nm, respectively. As the CTGF-loaded sheath-core nanofibers exhibited a similar size to that of pristine PLGA nanofibers, the incorporation of pharmaceuticals led to a significant reduction in the dimension of electrospun nanofibers (Fig. 5B) ($p < 0.05$). During the electrospinning process, the polymer plays a role in resisting the external stretching force exerted by the electric field. The presence of pharmaceuticals in the nanofibers reduced the PLGA percentage, weakening the fibers' ability to resist the electric stretching force during electrospinning, which consequently led to a smaller fiber size.

Fig. 6 illustrates the measured wetting angles of electrospun and co-electrospun nanofibers. While the pristine PLGA nanofibers and the sheath-core structured CTGF loaded nanofibers exhibited hydrophobic characteristics, the incorporation of

water-soluble pharmaceuticals (teicoplanin, ceftazidime, and ketorolac) substantially increased the hydrophilicity of the spun nanofibers ($p < 0.05$).

Fig. 7A shows the FTIR spectra of pristine PLGA and pharmaceuticals embedded PLGA nanofibers. The vibration peaks at $2870–2960$ cm^{-1} and $1650–1700$ cm^{-1} were promoted due to the $-CH_3$ and $C=O$ bonds of the loaded pharmaceuticals.[30–32] The new vibration peak at $1550–1600$ cm^{-1} was mainly owing to the N–H bonds of teicoplanin/ceftazidime/ketorolac. Meanwhile, the vibration peak at $1500–1530$ cm^{-1} was mainly resulted from the $C=C$ bond of incorporated drugs. Fig. 7B displays the DSC thermogram of pristine PLGA and pharmaceutical-loaded PLGA nanofibers. The exothermal peaks near 131 °C, relating to ceftazidime,[33] the peak near 120 °C corresponding to teicoplanin,[30] and the peaks near 160 and 170 °C corresponding to ketorolac,[34] could be found. All peaks almost diminished after being embedded into the PLGA matrix. The experimental results
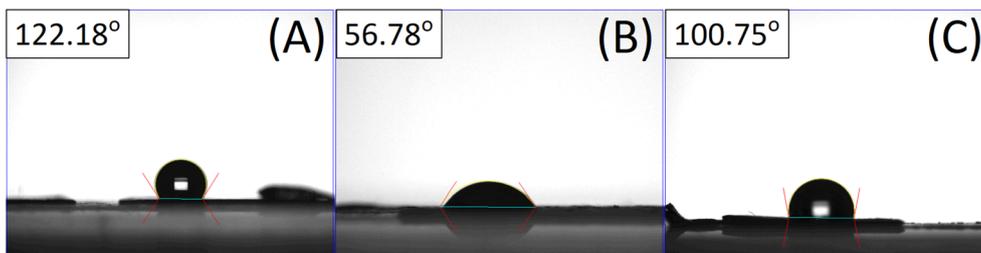
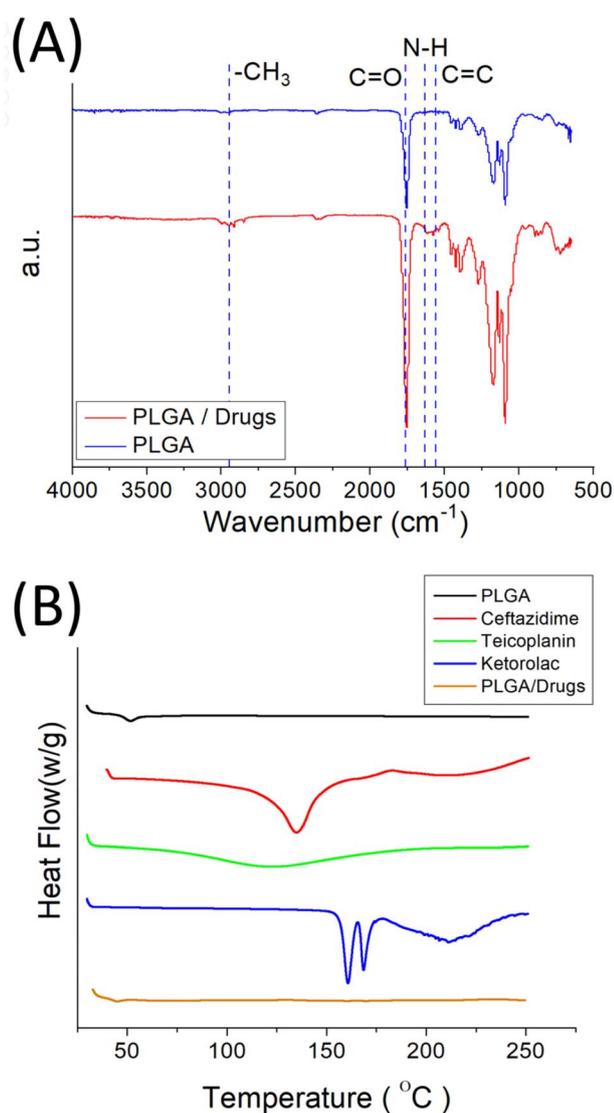Fig. 6 Wetting angles of (A) virgin PLGA nanofibers, (B) drugs loaded nanofibers, (C) CTGF loaded nanofibers.

Fig. 7 (A) FTIR spectra, (B) DSC thermograms of virgin PLGA and drugs (ceftazidime, teicoplanin, and ketorolac) loaded PLGA nanofibers.

Fig. 8 *In vitro* (A) daily and (B) cumulative release of teicoplanin, ceftazidime, and ketorolac, as well (C) daily discharge of CTGF from the nanofibers.

demonstrate that the drugs were successfully incorporated into the PLGA nanofibers.

3.2 *In vitro/in vivo* elution

Fig. 8A and B illustrate the *in vitro* daily and cumulative release patterns of teicoplanin, ceftazidime, and ketorolac from the
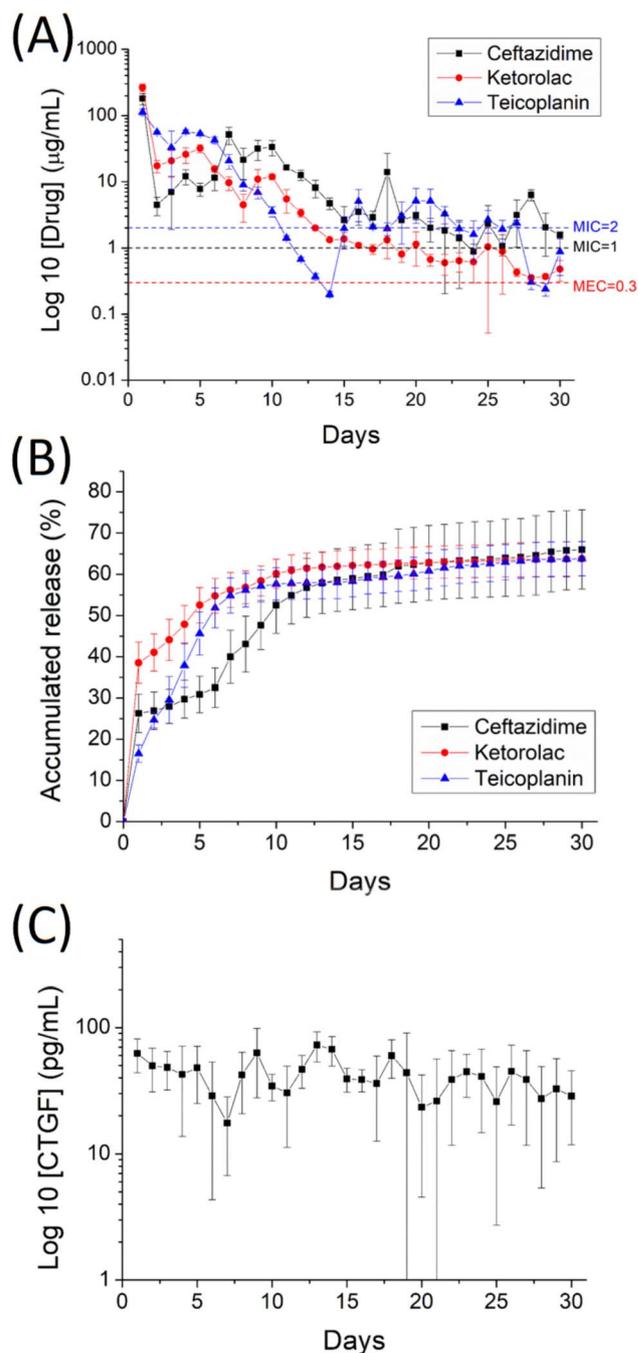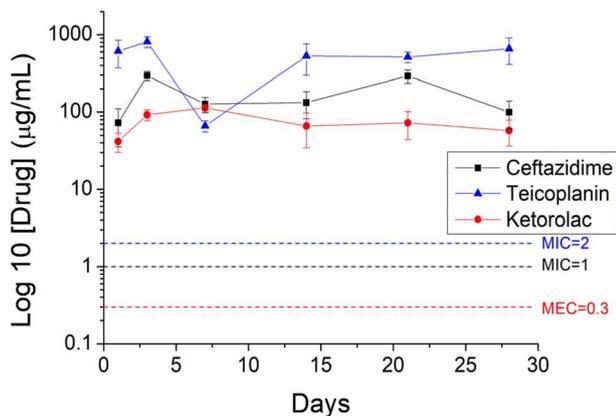
Fig. 9 *In vivo* elution of teicoplanin, ceftazidime, and ketorolac from the drug-eluting nanofibrous pads.

nanofibers. All three drugs displayed an initial burst release on the first day. Following this, teicoplanin showed minor peak discharges between days 15 and 27. Ceftazidime, in contrast, displayed secondary peaks at days 7, 10, and 17, followed by a gradual decline in release. Meanwhile, ketorolac demonstrated peak releases on days 5 and 10 after the initial burst, then continued a steady, gradually decreasing elution up to 30
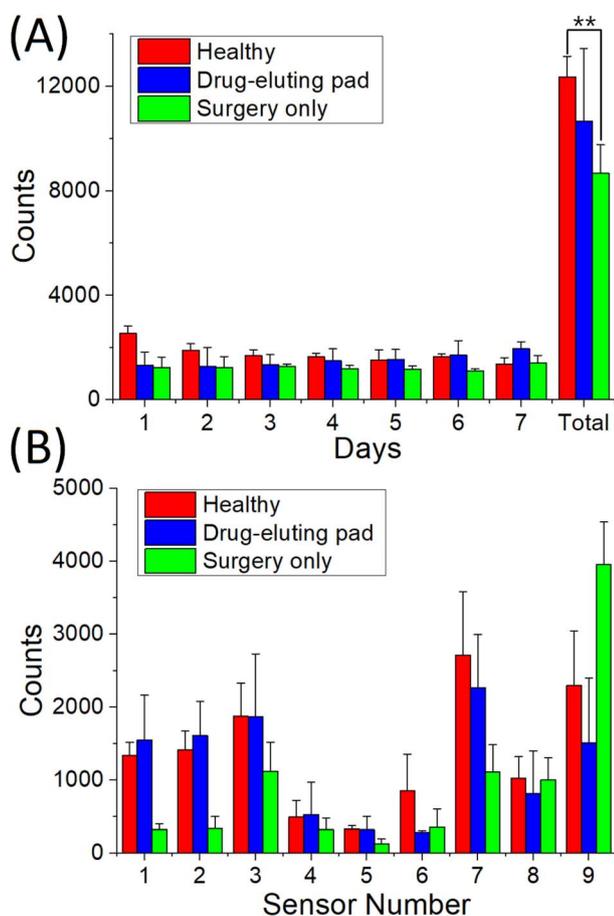
days. Overall, the drug-embedded nanofibers sustained the elution of high concentrations of teicoplanin, ceftazidime, and ketorolac for 10, 24, and 30 days, respectively. Additionally, Fig. 8C presents the release profile of CTGF from the sheath-core nanofibers. Due to the protective effect of the PLGA sheath, no initial burst release was observed. Furthermore, the co-electrospun nanofibers maintained high levels of CTGF release for over 30 days.

Fig. 9 illustrates the release profiles of drugs from the drug-eluting pads *in vivo*. The pads maintained high concentrations of teicoplanin, ceftazidime, and ketorolac at the rabbit knee joints for over 28 days, with levels exceeding the minimum inhibitory concentration for teicoplanin and ceftazidime and the minimum effective concentration for ketorolac.

3.3 Post implantation activity and histology assay

Fig. 10a displays the activity counts of the three groups over the 1-week postoperative period, while Fig. 10b shows the counts recorded by different sensors. Rabbits in all groups exhibited higher trigger counts at sensors 3 and 7, corresponding to the locations of food and water supply. The number of triggers at all other sensors exceeded that of sensor 5 at the center, indicating more frequent position changes along the cage's wall. Additionally, the total trigger counts obtained from the photoelectric switch sensors were $12\,358 \pm 790$, $10\,671 \pm 2776$, and 8668 ± 1098 for the healthy group, drug-eluting pad group, and surgery-only group, respectively. Rabbits in the surgery-only group showed significantly lower post-implantation activity compared to the healthy group ($p < 0.01$), mainly due to pain resulting from the surgical trauma. Animals receiving the implantation of drug/biomolecule-eluting pads exhibited higher activity counts than the surgery-only group, although the difference was not statistically significant ($p > 0.05$). Furthermore, animals implanted with drug/biomolecule-eluting pads demonstrated comparable activity to the healthy group ($p > 0.05$), confirming the effectiveness of the drug-eluting pads in promoting rabbit activity.

Fig. 11 displays the histological images at 1, 7, 14, and 28 days post-implantation. Microscopic examination of the tissue on day 7 revealed significant mononuclear cell infiltration, including lymphocytes, plasma cells, and eosinophils, following surgery. The number of polymorphonuclear leukocytes gradually decreased over time, up to day 28 post-surgery.

4 Discussion

HA is naturally present in various tissues and bodily fluids, with the highest concentrations found in articular cartilage and synovial fluid. It is a non-sulfated, naturally occurring glycosaminoglycan (GAG) with unique physicochemical properties, synthesized by synoviocytes, fibroblasts, and chondrocytes.[13,14] HA plays a crucial role in maintaining the biomechanics of healthy synovial fluid by enhancing lubrication and viscoelasticity. However, as osteoarthritis progresses with aging, both HA concentration and molecular weight decrease. Intra-articular HA injections involve delivering hyaluronic acid directly into
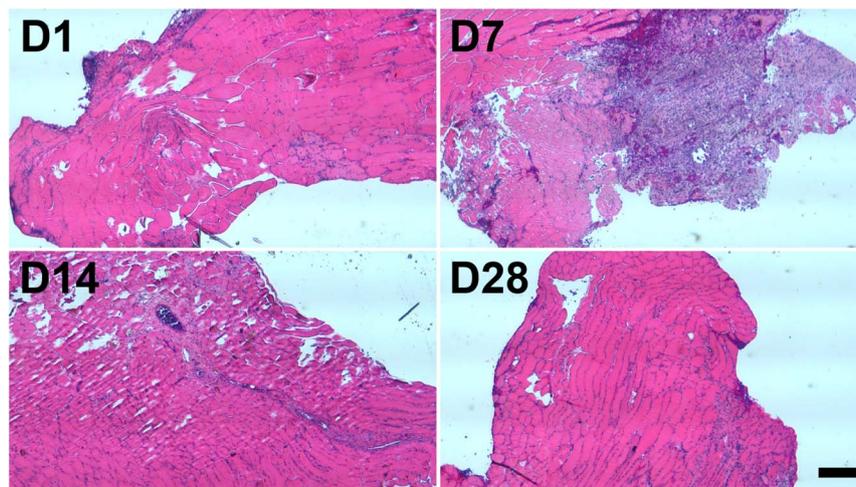

Fig. 10 Activity counts of animals (A) on various days, and (B) at different sensor locations (**, $p < 0.01$).

Fig. 11 Microscopic images of hematoxylin-and-eosin-stained tissue samples collected from the suprapatellar pouch of the knee joint at 1, 7, 14, and 28 days post-surgery (scale bar: 500 μm).

the affected joint to improve lubrication, cushion the joint, alleviate pain, and enhance function. This treatment is particularly beneficial for knee osteoarthritis, as it provides mechanical viscosupplementation, facilitating lubrication and shock absorption, while also promoting joint homeostasis by stimulating endogenous HA production.[35]

However, the disadvantage of intra-articular HA for arthritis treatment lies in that its effects may be temporary and not long-lasting for all patients. While some patients may experience significant pain relief and improved joint function after intra-articular HA, others may find that the benefits wear off over time, requiring repeated injections for sustained relief. Additionally, HA injections may not be effective for all types of arthritis or in advanced stages of the disease.[36] Some patients may not respond well to the treatment or may experience adverse reactions such as pain, swelling, or infection at the injection site.

In this study, we successfully developed antibiotics, analgesics, and CTGF-incorporated nanofibrous degradable HA pads, with PCL as the outer casing of the pads and PLGA as the delivery vehicle using co-axial electrospinning techniques. The HA loaded drug-eluting nanofibrous pad offers several advantages in the treatment of degenerative arthritis. Firstly, it provides cushioning effect on joints affected by degenerative arthritis. HA is a naturally present compound in the synovial fluid of joints, known for its ability to provide lubrication and cushioning to the articular surfaces. By incorporating HA into the nanofibrous pad, it enhances the cushioning effect within the joint space, reducing friction between the bones and mitigating pain associated with arthritis. This cushioning effect helps to distribute mechanical loads evenly across the joint, thereby relieving pressure on damaged cartilage and promoting joint mobility. Additionally, the drug-eluting properties of the nanofibrous pad allow for the controlled release of pharmaceutical agents, such as antibiotics, analgesics, and growth factors, directly to the affected joint. This targeted delivery system ensures that the therapeutic agents remain localized,

maximizing their efficacy while minimizing systemic side effects. Additionally, the pad can be tailored to release multiple drugs simultaneously, addressing various aspects of arthritis pathology, such as infection control, pain management, and tissue regeneration. Furthermore, the biodegradable nature of the pad ensures that it gradually degrades over time, eliminating the need for surgical removal. This feature promotes tissue integration and reduces the risk of foreign body reactions.

The experimental data confirm that the pharmaceutical-eluting nanofibrous pads extendedly discharged effective teicoplanin, ceftazidime, and ketorolac for 10, 24 and 30 days, respectively, and discharged high concentrations of CTGF for a period of 30 days. The *in vivo* animal test shows the pads also eluted high levels of antibiotics and analgesic for 28 days in a rabbit knee joint model, which is beneficial for managing infections and pain. The PCL pads also displayed good mechanical property and excellent biocompatibility. The animals receiving the implantation of drugs/biomolecules-eluting pads exhibited comparable activity with those receiving no surgeries.

Typically, drug release from a biodegradable pharmaceutical-embedded device occurs in three distinct phases: an initial peak release, diffusion-driven elution, and degradation-controlled discharge.[37,38] In drug-loaded nanofibers, most pharmaceuticals are encapsulated within the PLGA fibers after electrospinning. However, some drugs may be distributed on the nanofiber surfaces, contributing to the initial peak release. After the burst, the integrated influence of drug diffusion and polymer matrix degradation led to the second peak of drug release, namely at 16–21, 17, and 9–10 days, respectively, for teicoplanin, ceftazidime, and ketorolac. Thereafter, the PLGA degradation dominated the discharge behavior and the nanofibers demonstrated a sustained and progressively decreasing release of the embedded pharmaceuticals.[39] The experimental data also demonstrated that the pad provided slower and more sustained *in vivo* drug release

compared to the *in vitro* environment. This is because the *in vivo* release of drugs from nanofibers is influenced by biological barriers such as tissue, cellular membranes, and extracellular matrix components. These barriers can slow the diffusion of the drug compared to *in vitro* conditions, where such barriers are absent. Biological fluids also have distinct properties, such as viscosity, pH, and ionic strength, which can further affect drug release rates.

Localized and topical delivery of pharmaceuticals or biomolecules to target tissues ensures high and sustained local concentrations while avoiding the need for large systemic doses, thereby reducing the risk of systemic side effects such as hypoglycemia. Our previous studies[40,41] demonstrated that when a nanofibrous local drug delivery system is used, systemic drug concentrations in the blood remain significantly lower than those at the target site, offering the advantage of minimized systemic toxicity. However, while the sustained release of antibiotics such as teicoplanin and ceftazidime provides clear benefits in maintaining localized antibacterial activity and limiting systemic exposure, it also raises concerns about the potential development of bacterial resistance.[42,43] Prolonged exposure to antibiotics, especially at subtherapeutic concentrations as the release rate declines over time, can create selective pressure that promotes the emergence of resistant bacterial strains.

On the other hand, when the biomolecules were introduced to the core of electrospun sheath-core nanofibers, owing to the protective influence of the sheath polymeric layer, no initial peak release was observed. All these findings suggest that pharmaceuticals and biomolecules-loaded biodegradable pads can serve as an effective scaffold for treatment of degenerative arthritis.

This preliminary work had certain limitations. First, the study employed a knee joint model in healthy rabbits and confirmed the sustained release of drugs and biomolecules at the target site. However, a diseased model with a larger number of animals exhibiting degenerative arthritis should be used to further validate the effectiveness of the hybrid drug-eluting pads. In this study, we demonstrated that effective drug concentrations were achieved initially; however, we did not directly evaluate the long-term antibacterial efficacy or the potential development of resistance following prolonged exposure. Future investigations should assess bacterial susceptibility after exposure and evaluate resistance development in both acute and chronic infection models. Although the pad was capable of releasing high levels of CTGF for 30 days *in vitro*, the *in vivo* efficacy of CTGF over such an extended period still requires verification. Additionally, cartilage in rabbits is significantly thinner than in humans, which can affect the penetration, retention, and distribution of locally delivered drugs. Therefore, direct scaling of dosage and delivery system size must be approached with caution, often necessitating dose adjustments or modifications to the delivery strategy for human applications. Future studies will explore these aspects in greater detail.

5 Conclusions

We developed hyaluronic acid loaded drug-eluting nanofibrous pad. The empirical data show that the degradable pad exhibited good mechanical property. The drug-eluting nanofibrous pad also extendedly discharged effective teicoplanin, ceftazidime, and ketorolac for 10, 24 and 30 days, respectively, and discharged high levels of connective tissue growth factor for 30 days. In addition, the animal test shows the drug-eluting nanofibrous pad eluted high levels of antimicrobial and pain-relieving agents for over 28 days in a rabbit knee joint model. The animals receiving the implantation of drugs/biomolecules-eluting pads exhibited comparable activity with the animals receiving no surgery. The findings in this study suggested that the biodegradable drug-eluting pads with prolonged release of antimicrobial agents, analgesics, and growth factors have promising applications for therapy of degenerative arthritis as well as for post-surgical infection and pain management.

Data availability

All data of this work have been included in the manuscript.

Conflicts of interest

The authors state that there are no conflicts of interest.

Acknowledgements

References

1 L. A. Salman, G. Ahmed, S. G. Dakin, B. Kendrick and A. Price, Osteoarthritis: a narrative review of molecular approaches to disease management, *Arthritis Res. Ther.*, 2023, **25**, 27.

2 Y. Cho, S. Jeong, H. Kim, D. Kang, J. Lee, S. B. Kang and J. H. Kim, Disease-modifying therapeutic strategies in osteoarthritis: current status and future directions, *Exp. Mol. Med.*, 2021, **53**, 1689–1696.

3 M. Maqbool, G. Fekadu, X. Jiang, F. Bekele, T. Tolossa, E. Turi, G. Fetensa and K. Fanta, An up to date on clinical prospects and management of osteoarthritis, *Ann. Med. Surg.*, 2021, **72**, 103077.

4 A. Latourte, M. Kloppenburg and P. Richette, Emerging pharmaceutical therapies for osteoarthritis, *Nat. Rev. Rheumatol.*, 2020, **16**, 673–688.

5 M. Panikkar, E. Attia and S. Dardak, Osteoarthritis: a review of novel treatments and drug targets, *Cureus*, 2021, **13**(11), e20026.

6 B. Abramoff and F. E. Caldera, Osteoarthritis: pathology, diagnosis, and treatment options, *Med. Clin. North Am.*, 2020, **104**(2), 293–311.

7 Y. Liu, K. M. Shah and J. Luo, Strategies for articular cartilage repair and regeneration, *Front. Bioeng. Biotechnol.*, 2021, **9**, 770655.

8 K. Jain and P. Ravikumar, Recent advances in treatments of cartilage regeneration for knee osteoarthritis, *J. Drug Delivery Sci. Technol.*, 2020, **60**, 102014.

9 X. Guo, L. Xi, M. Yu, Z. Fan, W. Wang, A. Ju, Z. Liang, G. Zhou and W. Ren, Regeneration of articular cartilage defects: Therapeutic strategies and perspectives, *J. Tissue Eng.*, 2023, **14**, 1–27.

10 N. Bhardwaj, D. Devi and B. B. Mandal, Tissue-engineered cartilage: the crossroads of biomaterials, cells and stimulating factors, *Macromol. Biosci.*, 2015, **15**(2), 153–182.

11 M. Fallah Tafti and S. Faghihi, Cartilage Tissue Engineering: Advances and Frontiers, in *Cartilage: from Biology to Biofabrication*, ed., M. Baghaban Eslaminejad, S. Hosseini. Springer, Singapore, 2023.

12 S. Vasvani, P. Kulkarni and D. Rawtani, Hyaluronic acid: A review on its biology, aspects of drug delivery, route of administrations and a special emphasis on its approved marketed products and recent clinical studies, *Int. J. Biol. Macromol.*, 2020, **151**(15), 1012–1029.

13 R. C. Gupta, R. Lall, A. Srivastava and A. Sinha, Hyaluronic acid: molecular mechanisms and therapeutic trajectory, *Front. Vet. Sci.*, 2019, **6**, 192.

14 A. Migliore and S. Procopio, Effectiveness and utility of hyaluronic acid in osteoarthritis, *Clin. Cases Miner. Bone Metab.*, 2015, **12**(1), 31–33.

15 E. Maheu, F. Rannou and J.-Y. Reginster, Efficacy and safety of hyaluronic acid in the management of osteoarthritis: Evidence from real-life setting trials and surveys, *Semin. Arthritis Rheum.*, 2016, **45**(4), S28–S33.

16 M. Labet and W. Thielemans, Synthesis of polycaprolactone: a review, *Chem. Soc. Rev.*, 2009, **38**(12), 3484–3504.

17 R. Pawar, A. Pathan, S. Nagaraj, H. Kapare, P. Giram and R. Wavhale, Polycaprolactone and its derivatives for drug delivery, *Polym. Adv. Technol.*, 2023, **34**(10), 3296–3316.

18 D. N. Kapoor, A. Bahtia, R. Kaur, R. Sharma, G. Kaur and S. Dhawan, PLGA: a unique polymer for drug delivery, *Ther. Deliv.*, 2015, **6**(1), 41–58.

19 S. Marquina, M. Ozgul, K. Robertson-Brown and M. C. Kenney, A review on PLGA particles as a sustained drug-delivery system and its effect on the retina, *Exp. Eye Res.*, 2023, **235**, 109626.

20 Y. Su, B. Zhang, R. Sun, W. Liu, Q. Zhu, X. Zhang, R. Wang and C. Chen, PLGA-based biodegradable microspheres in drug delivery: recent advances in research and application, *Drug Deliv.*, 2021, **28**(1), 1397–1418.

21 F. Khamesipour, S. M. Hashemian, A. A. Velayati and P. Tabarsi, A review of teicoplanin used in the prevention and treatment of serious infections caused by Gram-positive bacteria and compared its effects with some other antibiotics, *Biomed. Pharmacol. J.*, 2015, **8**(1), 513–521.

22 D. M. Richards and R. N. Brogden, Ceftazidime. A review of its antibacterial activity, pharmacokinetic properties and therapeutic use, *Drugs*, 1985, **29**(2), 105–161.

23 T. E. Mallinson, A review of ketorolac as a prehospital analgesic, *J. Paramedic Pract.*, 2017, **9**(12), 522–526.

24 Z. Chen, N. Zhang, H. Y. Chu, Y. Yu, Z. K. Zhang, G. Zhang and B. T. Zhang, Connective tissue growth factor: from molecular understandings to drug discovery, *Front. Cell Dev. Biol.*, 2020, **8**, 593269.

25 J. Xue, T. Wu, Y. Dai and Y. Xia, Electrospinning and electrospun nanofibers: Methods, materials, and applications, *Chem. Rev.*, 2019, **119**(8), 5298–5415.

26 D. Ji, Y. Lin, X. Guo, B. Ramasubramanian, R. Wang, N. Radacsi, R. Jose, X. Qin and S. Ramakrishna, Electrospinning of nanofibres, *Nat. Rev. Methods Primers*, 2024, **4**, 1.

27 P. Rathore and J. D. Schiffman, Beyond the single-nozzle: Coaxial electrospinning enables innovative nanofiber chemistries, geometries, and applications, *ACS Appl. Mater. Interfaces*, 2021, **13**(1), 48–66.

28 Y. H. Yu, S. J. Shen, Y. H. Hsu, Y. C. Chou, P. C. Yu and S. J. Liu, Tri-layered doxycycline, collagen and bupivacaine loaded poly(lactic-co-glycolic acid) nanofibrous scaffolds for tendon rupture repair, *Polymers*, 2022, **14**, 2659.

29 C. H. Lee, D. Y. Chen, M. J. Hsieh, K. C. Hung, S. C. Huang, C. J. Cho and S. J. Liu, Nanofibrous insulin/vildagliptin core-shell PLGA scaffold promotes diabetic wound healing, *Front. Bioeng. Biotechnol.*, 2023, **11**, 1075720.

30 S. A. Kahdestani, M. H. Shahriari and M. Abdouss, Synthesis and characterization of chitosan nanoparticles containing teicoplanin using sol–gel, *Polym. Bull.*, 2021, **78**, 1133–1148.

31 L. R. Osório, A. B. Meneguin, H. B. da Silva, H. M. Barreto, J. A. Osajima and E. C. da Dilva Filho, Evaluation of physico-chemical properties and antimicrobial synergic effect of ceftazidime-modified chitosan, *J. Therm. Anal. Calorim.*, 2018, **134**, 1629–1636.

32 B. Amul, S. Muthu, M. Raja and S. Sevvanthi, Molecular structure, spectroscopic (FT-IR, FT-Raman, NMR, UV-VIS), chemical reactivity and biological examinations of Ketorolac, *J. Mol. Struct.*, 2020, **1210**, 128040.

33 M. S. de Santana, Y. S. de Oliveira, W. C. Ferreira, V. S. Neto and A. P. Ayala, Stability of ceftazidime pentahydrate investigated by thermal analysis techniques, *J. Pharm. Sci.*, 2020, **109**(3), 1324–1329.

34 Y. T. Sohn and H. O. Seo, Crystal forms of ketorolac, *Arch Pharm. Res.*, 2004, **27**(3), 357–360.

35 I. A. Jones, R. Togashi, M. L. Wilson, N. Heckmann and Jr C. T. Vangsness, Intra-articular treatment options for knee osteoarthritis, *Nat. Rev. Rheumatol.*, 2019, **15**, 77–90.

36 S. Charda, S. A. Rabbani and T. Wadhwa, Role and effectiveness of intra-articular injection of hyaluronic acid in the treatment of knee osteoarthritis: a systematic review, *Cureus*, 2022, **14**(4), e24503.

37 S. Fredenberg, M. Wahlgren, M. Reslow and A. Axelsson, The mechanisms of drug release in poly(lactic-co-glycolic acid)-based drug delivery systems-a review, *Int. J. Pharm.*, 2011, **415**(1–2), 34–52.

38 D. J. Hines and D. L. Kaplan, Poly (lactic-co-glycolic acid) controlled release systems: experimental and modeling

insights, *Crit. Rev. Ther. Drug Carrier Syst.*, 2013, **30**(3), 257–276.

39 H. K. Makadia and S. J. Siegel, Poly lactic-co-glycolic acid (PLGA) as biodegradable controlled drug delivery carrier, *Polymers*, 2011, **3**(3), 1377–1397.

40 Y. P. Chen, T. S. Lo, Y. H. Chien, Y. H. Kuo and S. J. Liu, In vitro and in vivo drug release from a nano-hydroxyapatite reinforced resorbable nanofibrous scaffold for treating female pelvic organ prolapse, *Polymers*, 2024, **16**, 1667.

41 C. J. Weng, Y. C. Wu, M. Y. Hsu, F. P. Chang and S. J. Liu, Electrospun, resorbable, drug-eluting, nanofibrous membranes promote healing of allograft tendons, *Membranes*, 2022, **12**, 529.

42 O. Yushchuk, B. Ostash, A. W. Truman, F. Marinelli and V. Fedorenko, Teicoplanin biosynthesis: unraveling the interplay of structural, regulatory, and resistance genes, *Appl. Microbiol. Biotechnol.*, 2020, **104**, 3279–3291.

43 Y. Wang, M. Sholeh, L. Yang, M. Z. Shakourzadeh, M. Beig and K. Azizian, Global trends of ceftazidime–avibactam resistance in gram-negative bacteria: systematic review and meta-analysis, *Antimicrob. Resist. Infect. Control*, 2025, **14**, 10.